09

Dispersion properties of nano- and micropores in track membranes

© A.V. Mitrofanov, R.M. Feshchenko

Lebedev Physical Institute, Russian Academy of Sciences,
119991 Moscow, Russia
e-mail: rusl@sci.lebedev.ru

Received May 6, 2024
Revised May 6, 2024
Accepted May 6, 2024

A theoretical explanation of the constancy of the phase and group velocities of waves in through pores of polymer track membranes in the hard X-ray range, which was discovered in earlier works and not satisfactory explained by the theory of waveguide modes, is proposed. The developed X-ray propagation theory is based on the analytical solution of the parabolic equation in a waveguide by an integral transformation method. Using the 3*D* parabolic equation and a finite-difference method a numeric simulation of the X-ray propagation at two soft X-ray wavelengths was conducted, which demonstrated that the constancy of the phase and group velocities in through pores of track membranes holds in this case as well but with a lower precision. However, the product of the phase and group velocities is not equal to the square of the vacuum light speed anymore. It was also shown that constancy of the wave velocities in a pore breaks down when several propagating waveguides modes appear in it, which leads to oscillations of the wave velocities due to modes' interference.

Keywords: X-ray filters, 3*D* parabolic equation, finite-difference method, waveguide modes, track membranes.

DOI: 10.61011/TP.2024.07.58814.157-24

Introduction

Thin polymer track membranes with micron or submicron through pores [1] have a variety of applications as soft X-ray and extreme ultraviolet ($1 < \lambda < 100$ nm) optics components [2–6]. As an example, the track membranes are used as detector filters in solar telescopes (for example, in the Koronas-F project X-ray telescope [4]) for protection of the radiation detector against intense exposure to long-wavelength radiation from an object of interest, e.g. the Sun, as well as against UV, visible and IR band instrument glare.

It is known that phase characteristics of track membranes depend on pore geometry, incident light wavelength and optical properties of the membrane material. One of the understudied issues is understanding of how the wave field phase changes after propagation through a porous track membrane. This is important for the development of phase filters and phase screens for X-ray radiation based on track membranes, e.g. those to be used as test objects in phase X-ray microscopy. In [7,8], it was shown that the wave phase portrait repeats the pore geometry after propagation of the hard X-ray radiation through a pore with quite a large diameter, while considerable transverse phase smearing was observed or small-diameter pores. It is also demonstrated that detected phase smearing is described by the universal Fresnel number function for a single pore. Numerical simulations make it possible to advance the use of track membranes as X-ray diffusors and for suppression of speckles in coherent imaging optical systems. Note, however, that [7,8] performed numerical simulation of the X-ray radiation propagation in pores on the assumption of strict cylindrical symmetry of a 2*D*-parabolic approximation problem using one-dimensional finite-difference scheme and one-dimensional exact boundary condition, which is an approximation even for a cylindrical symmetry problem. These studies also did not calculate explicitly the phase and group velocities of waves in pores and their properties were discussed only qualitatively.

Therefore the behavior of phase and group [9] velocities of X-ray radiation propagating in narrow pores of polymer track membranes is of considerable interest. Due to membrane material dispersion, both phase and group velocities of waves in a hollow X-ray micro- or nanowaveguide such as a through pore will depend in a complicated way on the pore diameter, radiation wavelength and pore length. They may also depend on the surface roughness of pore walls. Practical interest in the phase and group velocity behavior in track membrane pores is associated with the fact that their dispersion may affect the temporal shape of a short X-ray pulse going through a porous membrane. X-ray lasers or free-electron lasers, for example, may serve as sources of such short pulses [10].

The goal of the study is to perform numerical simulation of soft X-ray propagation in through pores in thin polyethylene terephthalate (PET) track membranes as has been already done before for hard X-ray radiation in [11]. Phase and group velocity behavior in pores and their variation depending on the pore diameter and X-ray wavelength will be examined. Ultimately, analytical theory of radiation propagation in a planar (for simplicity) waveguide will be presented and qualitative interpretation of the phase and group velocity constancy and weak dependence on the pore diameter (in hard X-ray range) will be provided on the basis of the theory.

1. Phase and group velocities

Plane wave propagation in a arbitrary medium is generally characterized by two velocities: phase v_{ph} and group v_{gr} (see [12] paragraphs 38 to 39). The former reflects the field phase variation rate in the specified direction (for example, in the z axis direction) and is defined as

$$v_{ph} = \frac{\omega}{k_z} = \frac{\omega}{\mathrm{Im}\frac{\partial}{\partial z}(\ln E)}, \quad (1)$$

where E is the electric field of wave, ω is the wave frequency and k_z is the wave vector component in the z axis direction. If the wave field is written as $E = u \cdot \exp(-i\omega t + ikz)$, where the wave number $k = \omega/c$, c is the speed of light in vacuum and u is the field amplitude, then it follows from (1) that

$$v_{ph} = \frac{\omega}{k_z} = \frac{c}{1 + \frac{1}{k}\mathrm{Im}\frac{\partial}{\partial z}(\ln u)}. \quad (2)$$

Unlike the phase velocity, the group velocity describes the mean velocity of wave packet motion (if the spectrum width is not too high) and may be calculated using the Rayleigh equation [12], if the dependence of phase velocity on the radiation wavelength is known as

$$v_g = v_{ph} - \lambda\frac{\partial v_{ph}}{\partial \lambda}, \quad (3)$$

where $\lambda = 2\pi/k$ is the X-ray radiation wavelength. Both velocities may be found by means of numerical solution of the problem of radiation propagation in porous medium followed by the use of equations (1) or (2) and then (3).

2. Numerical simulation

The study uses 3D-parabolic equation to simulate X-ray radiation propagation

$$2ik\frac{\partial u}{\partial z} = -\frac{\partial^2 u}{\partial x^2} - \frac{\partial^2 u}{\partial y^2} - k^2(\varepsilon(x,y) - 1)u, \quad (4)$$

where $u(x,y,z)$ is the slowly varying field amplitude, (x,y,z) are the Cartesian coordinates, $\varepsilon(x,y) = n^2 \approx \approx 1 - 2\delta + 2i\beta$ is the complex dielectric permittivity of a material medium (PET polymer herein). Equation (4) is solved using the explicit-implicit unconditionally stable Crank–Nicolson finite-difference scheme with exact transparent boundary conditions in a rectangular computational domain. A rectangular uniform computational grid with a longitudinal (on z) step τ which is much higher than the transverse space h (on the x and y coordinates) is used. The employed numerical methods and transparent boundary conditions are described in detail in [11,13,14].

All calculations were carried out using software codes developed specially for this purpose in Matlab. Optical constants of PET are taken from the database [15] and are given in the table for the wavelengths described herein.

Optical constants of PET at the wavelengths of interest

Wavelength λ, nm	δ	β
0.154	$4.533 \cdot 10^{-6}$	$1.028 \cdot 10^{-8}$
1.625	$5.304 \cdot 10^{-4}$	$1.086 \cdot 10^{-4}$
17.06	$4.181 \cdot 10^{-2}$	$1.348 \cdot 10^{-2}$

Radiation propagation through a single pore is simulated in a rectangular computational domain with a transverse dimension higher than the pore diameter. The longitudinal step length is equal to $\tau = 20$ or 100 nm. The specimen with pore is exposed to a plane wave falling at an angle of incidence θ (in the (y, z) plane) to the left pore end. The complex field amplitude u as function of coordinates is the simulation result. The phase velocity is calculated below as a field phase variation velocity according to the obtained amplitude u using equation (2). The amplitude derivative on z is calculated as the amplitude difference on two successive steps of the finite-difference scheme divided by the step length τ. To calculate the group velocity using equation (3), radiation propagation is calculated for two close wavelengths with $\delta\lambda = 0.01 \cdot \lambda$ with constants also taken from [15]. After passing the pore area, simulation is continued in a free space using the same finite-difference scheme and the same grid steps as in the membrane, but using 3D-parabolic equation (4) with $\varepsilon = 1$.

The calculated phase and group velocities of the wave field with $\lambda = 0.154$ nm propagating in a cylindrical pore of $D = 30$ nm in diameter in a PET membrane of $L = 22.4\,\mu$m in thickness are shown in Figure 1 for the angle of incidence $\theta = 0$. Simulation in vacuum was continued over a distance of 30 μm from the right end of the pore. Grid step h on the (x, y) transverse coordinates counted from the pore axis is equal to 1 nm. Figure 1 shows that the phase velocity inside the pore and in its proximity exceeds the speed of light in vacuum and the group velocity is lower than the speed of light in vacuum. It is also shown that both velocities are constant throughout the most part of pore and in its proximity (except the initial area where transition processes are observed) suggesting a linear phase growth along the pore.

Dependence of the phase and group wave velocities on the pore diameter are also of interest. Such dependences are shown in Figure 2 and the velocities were taken at the pore axis at a distance of 20 μm from its left end. Figure 2 (left-hand) shows that both velocities weakly depend on the pore diameter and decrease (increase) slowly as the diameter increases. The nature of such velocity dependence on the pore diameter is discussed below. Also note that it follows from Figure 2 that the product of the phase and group velocities is equal to squared speed of light in vacuum.

Now proceeding to a softer X-ray radiation where absorption in the medium plays a significant role, we take a look at the results for $\lambda = 1.625$ nm. The calculated phase

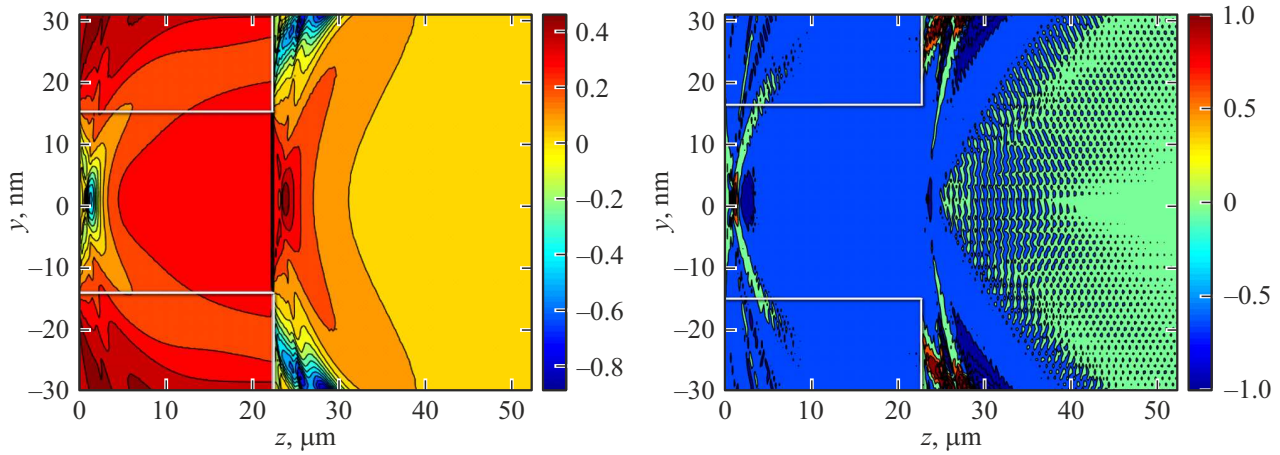

Figure 1. Phase $((v_{ph}/c - 1) \cdot 10^5$ — on the left) and group $((v_{gr}/c - 1) \cdot 10^5$ — on the right) velocities in the (y, z) plane for a wave at $\lambda = 0.154$ nm propagating in a narrow cylindrical pore. White lines correspond to the pore boundaries.

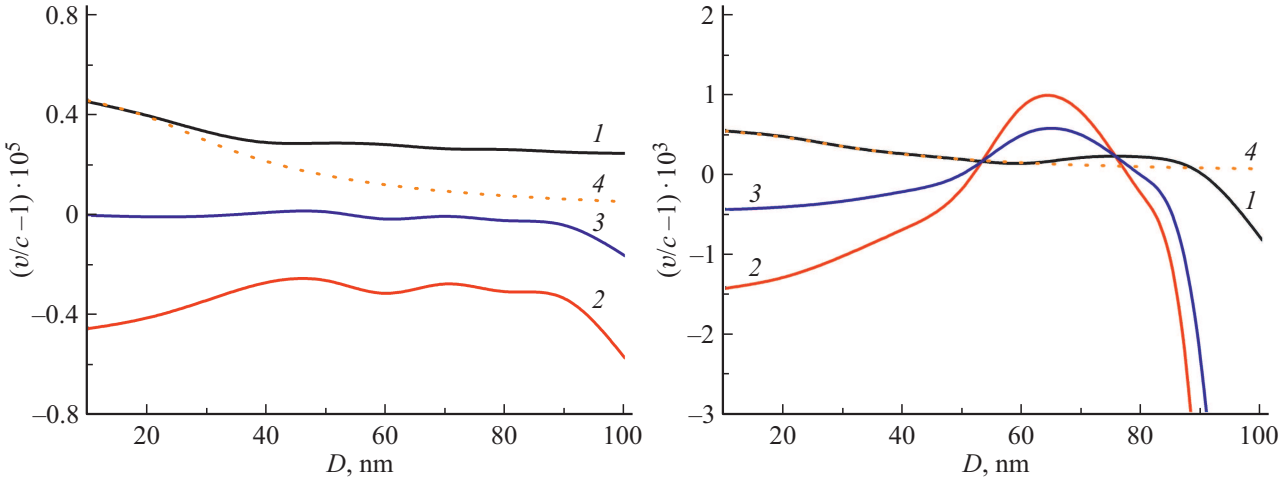

Figure 2. Phase (line *1*) and group (line *2*) velocities for a wave propagating in a cylindrical pore as function of the pore diameter. Left-hand — for $\lambda = 0.154$ nm, right-hand — for $\lambda = 1.625$ nm. Line *3* — the geometrical mean of the phase and group velocities. Line *4* — phase velocity for the fundamental waveguide mode calculated from (5).

and group velocities of the wave field with this wavelength propagating in a cylindrical pore of $D = 40$ nm in diameter in a PET membrane of $L = 8\,\mu$m in thickness are shown in Figure 3 for the angle of incidence $\theta = 0$. Simulation in vacuum was continued over a distance of $2\,\mu$m from the right end of the pore. The same grid step on the (x, y) transverse coordinates was chosen as before — 1 nm. With the chosen thickness, the membrane is opaque for X-ray radiation with $\lambda = 1.625$ nm.

Figure 3 shows that the phase velocity, like in the hard X-ray range, exceeds the speed of light in vacuum c and the group velocity is lower than the speed of light in vacuum. Note also that, though the phase and group velocities are approximately constant within the most part of the pore and in its proximity, they demonstrate oscillations around some mean value. This suggests almost linear phase growth along the pore. Thus, in the soft X-ray range, phase and group velocity behavior in quite narrow pores is similar to that at $\lambda = 0.154$ nm.

Nevertheless, changes in the velocity behavior compared with the hard X-ray radiation can be clearly seen in Figure 2 (to the right) that shows the dependences of phase and group velocities on the pore diameter for $\lambda = 1.625$ nm, whereas the velocities were taken on the pore axis at a distance of $7\,\mu$m from its left end. The figure shows that the phase velocity is still comparatively weakly depends on the pore diameter and decreases slightly as the diameter increases. While the dependence of the group velocity on the wavelength is non-monotonic and has a local peak at $D \approx 65$ nm. The product of the phase and group velocities is equal to squared velocity of light in vacuum. The reasons for such velocity behavior variation in the soft X-ray radiation range are discussed below.

As the last example, Figure 4 shows the calculated phase and group velocities of the wave field with $\lambda = 17.06$ nm

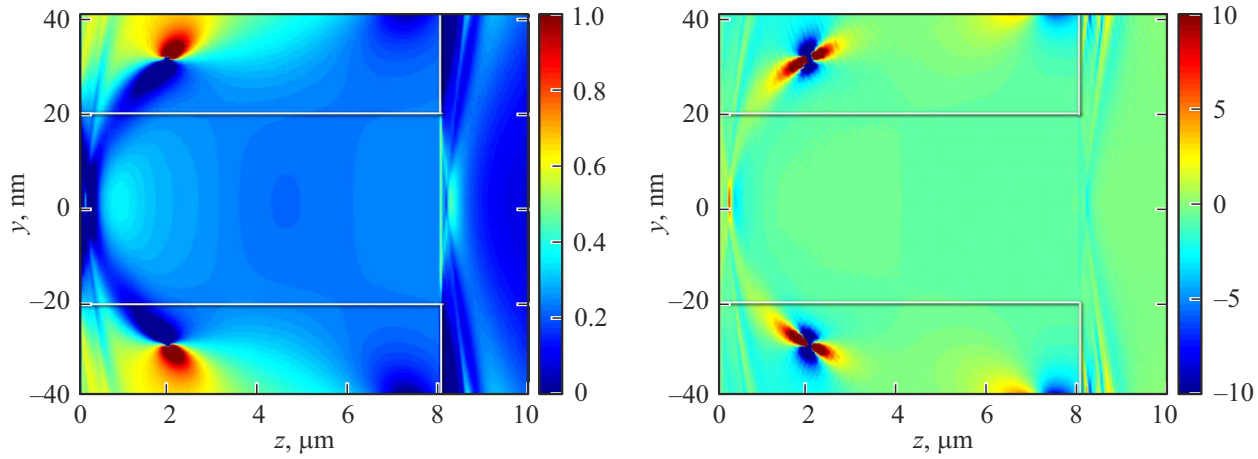

Figure 3. Phase $((v_{ph}/c - 1) \cdot 10^3$ — on the left) and group $((v_{gr}/c - 1) \cdot 10^3$ — on the right) velocities in the (y, z) plane for a wave at $\lambda = 1.625$ nm propagating in a narrow cylindrical pore. White lines correspond to the pore boundaries.

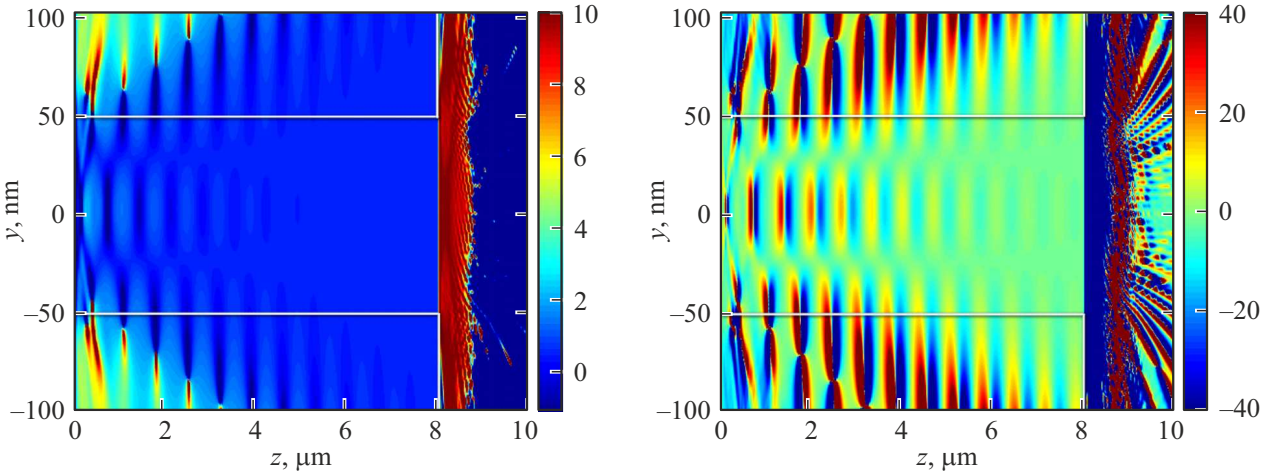

Figure 4. Phase $((v_{ph}/c - 1) \cdot 10^2$ — on the left) and group $((v_{gr}/c - 1 \cdot 10^2$ — on the right) velocities in the (y, z) plane for a wave at $\lambda = 17.06$ nm propagating in a narrow cylindrical pore. White lines correspond to the pore boundaries.

propagating in a cylindrical pore of $D = 100$ nm in diameter in a PET membrane of $L = 8\,\mu$m in thickness for the angle of incidence $\theta = 0$. The grid step on the (x, y) transverse coordinates was doubled up to $h = 2$ nm to reduce the computational costs. Simulation in vacuum was continued over a distance of $2\,\mu$m from the right end of the pore. With the chosen thickness the membrane, like in the previous example, is opaque for X-ray radiation.

Figure 4 shows that the phase velocity oscillates noticeably, but still exceeds the speed of light in vacuum c, whereas the group velocity oscillates strongly near a value equal to the speed of light in vacuum and no longer has a particular sign. The observed oscillations decay gradually with propagation in the pore. Such behavior of the group velocity differs from that for $\lambda = 1.625$ nm as shown in Figure 3.

The examples discussed above (Figure 1, 3 and 4) are calculated for the angle of incidence $\theta = 0$. Simulation for non-zero angles of incidence (in particular, for $\theta = 0.001$ at $\lambda = 0.154$ nm) has shown that the phase and group wave velocity behavior in narrow pores has no qualitative difference from that for the zero angle of incidence.

3. Findings and discussion

As is commonly known, for waveguide modes propagating in the cylindrical waveguide at small grazing angles with respect to the waveguide wall (like in the X-ray range), the Helmholtz scalar equation is approximately valid. Polarization effects in this case may be neglected due to the equality of reflectances of waves with different polarizations in grazing incidence.

Using the analytical solutions of the Helmholtz equation within the pore and polymer, a dispersion equation may be derived (taking into account the boundary conditions on the wall at $r = D/2$) for modes in the hollow cylindrical

waveguide (neglecting the absorption that is low in the hard X-ray range):

$$\kappa \frac{K'_m(\kappa D/2)}{K_m(\kappa D/2)} = \gamma \left(\frac{J'_m(\gamma D/2)}{J_m(\gamma D/2)}, \quad (5)$$

where m is the azimuthal index, γ is the transverse wave number for the mode in pore, $\kappa = \sqrt{k^2\delta - \gamma^2}$, K_m and J_m are the m-th order Macdonald function and Bessel function, respectively. Equation (5) is solved with respect to γ, while the phase velocity is expressed as $v_{ph} = ck/\sqrt{k^2 - \gamma^2}$. The group velocity may be still calculated using equation (3). Equation (5) is solved numerically by the iteration method. For this, a solution corresponding to the fundamental (axisymmetric) waveguide mode with $m = 0$ and $n = 1$ (radial number) is taken.

The phase velocity for the fundamental mode calculated according to equation (1) for $m = 0$ and $n = 1$ is shown in Figure 2 (line *4*) for two wavelengths corresponding to the hard (left-hand) and soft (right-hand) X-ray radiation. It can be seen that for small diameters $D < 30$ nm in the short-wavelength range, the solution of equation (5) matches well with the phase velocity of wave in the pore. However, the phase velocity of the fundamental waveguide mode at large pore diameters is much lower than the phase velocity calculated on the basis of the numerical solution of parabolic equation (4). The coincidence of the results obtained by the two calculation methods at low pore diameters may be explained by the fact that in this case the fundamental waveguide mode propagates mainly outside the pore. This means that the effective mode diameter is high compared with the pore diameter and therefore the phase and group velocities are defined only by the refraction index of the membrane material resulting in the coincidence of the two calculation methods. However, at large pore diameters, the wave phase velocity in the pore is much higher than the fundamental waveguide mode velocity meaning that radiation assigned not only to the fundamental waveguide mode propagates in the pore.

On the other hand, Figure 2 (right-hand) shows that a simple mode model of equation (5) in the long-wavelength range describes adequately the situation with pore diameters up to $D = 100$ nm. This may be explained by high medium absorption in this range because, as mentioned above, the $8\,\mu$m membrane is non-transparent for soft X-ray radiation. This results in significant loss of modes propagating through the pore and finally only the radiation of the fundamental mode having the minimum decay riches the right end of the pore. All higher modes, pseudo modes and radiation that is not assigned to a particular mode decay without reaching the right end of the pore. Complex group velocity behavior with a local peak (Figure 2, on the right-hand side) is explained by the complex behavoir of the PET optical constants in the soft X-ray range. In a softer range as shown in Figure 4, two modes propagate in the pore for the chosen diameter $D = 100$ nm and their interference results in the phase and group velocity oscillations that decay with propagation due to fast decay of the second mode compared with the fundamental mode.

To explain the wave velocity behavior in pores with a larger diameter in the hard range with $\lambda = 0.154$ nm, it is a good to use a simple model of a planar X-ray waveguide described by the $3D$-parabolic equation (4), where the amplitude u and dielectric permittivity ε of PET are assumed to be independent of the y coordinate. In this case, the equation may be solved using the integral Laplace transform on the longitudinal z coordinate:

$$F(x, p) = \int_0^\infty u(x, z) e^{-pz} dz,$$

when it is applied to equation (4), we get the following ordinary differential equation for F image:

$$\frac{d^2F}{dx^2} + (2ikp + k^2(\varepsilon(x) - 1))F = 2iku(x, 0). \quad (6)$$

The right-hand side of (6) contains the initial amplitude $u(x, 0)$ at $z = 0$ that is assumed to be equal to 1 herein. Equation (6) is solved considering the necessity to fulfil the radiation condition at $x \to \pm\infty$ and boundary conditions at $x = D/2$. Only symmetrical solutions are considered and the inverse Laplace transform is then applied to the obtained result. Finally, the field amplitude inside the planar waveguide at $-D/2 < x < D/2$ may be written as

$$u = 1 - \frac{\gamma_0^2}{\pi} \int_{-\sqrt{i\infty}}^{\sqrt{i\infty}} e^{-t^2} \frac{dt}{t\sqrt{t^2 - i\gamma_0^2}} \times \frac{\cos(\kappa_0 x)}{\sqrt{t^2 - i\gamma_0^2} \cdot \cos(\kappa_0 D/2) - it \sin(\kappa_0 D/2)}, \quad (7)$$

where the integral in equation (7) is taken along the contour on a complex plane above the real axis bypassing the poles and subintegral function branch points. By deforming this contour in such a way that the integration goes along the real axis changing to a new integration variable and summing the residuals in poles located in the upper half-plane, we get

$$u = \sum_{s=1}^{\infty} \frac{2}{w_s} e^{-i\gamma_0^2 w_s^2} \frac{\cos(2x\varsigma w_s/D)}{1 + \varsigma\sqrt{1 - w_s^2}} - \frac{\gamma_0^2}{\pi} e^{-i\gamma_0^2} \int_{-\infty}^{+\infty} \frac{e^{-\rho^2}}{\rho^2 + i\gamma_0^2} \times \frac{\cos(\kappa_0 x)}{\rho \cos(\kappa_0 D/2) - i\sqrt{\rho^2 + i\gamma_0^2} \sin(\kappa_0 D/2)} d\rho, \quad (8)$$

where $\gamma_0^2 = kz(\delta - i\beta)$, $\kappa_0^2 = 2k(\rho^2 + i\gamma_0^2)/(iz)$, $\varsigma = kD\sqrt{\delta - i\beta}/\sqrt{2}$. w_n is the dispersion equation solution for modes in the planar waveguide

$$\tan(\varsigma w_n) = \frac{\sqrt{1 - w_n^2}}{w_n}, \quad (9)$$

corresponding to the mode with $n \geq 1$. The first term in expression (8) is the sum of fields of various waveguide modes (and pseudo modes). The second term in (8) corresponds to the continuous spectrum and describes transition processes at the initial stage of radiation propagation in the membrane that are observed in Figure 1, 3, 4 in the form of complex field amplitude variations at small values of z. It may be shown that the intensity of this continuous spectrum generally decreases as $\sim 1/z$ with coordinate and at high z the contribution of this term becomes low compared with the propagating modes filed even in the hard X-ray radiation range where absorption is low.

As for the waveguide modes, they carry the finite radiation power and correspond to real (neglecting the absorption) solutions of (9) that satisfy $0 \leq w_n \leq 1$ and $\mathrm{tg}(\varsigma w_n) \geq 0$. These solutions correspond to zeros in the denominator of the second fraction in equation (7) lying on the straight line going out of zero with phase $3\pi/2$. The total number of modes is equal to $N = 1 + \lfloor \varsigma/\pi \rfloor$ and grows as the waveguide diameter increases. For $D < 100\,\mathrm{nm}$ and optical parameters from the table, one or two waveguide modes will propagate in the pore. As mentioned above, propagation of two waveguide modes takes place in a pore with $D = 100\,\mathrm{nm}$ at $\lambda = 17.06\,\mathrm{nm}$ (Figure 4), where their interference results in evident oscillations of the phase and group velocities. The mode fields propagate with a phase velocity lower than the wave velocity in a continuous medium as it follows from the structure of the exponent indexes in the sum in expression (8) and from condition $w_n \leq 1$.

In addition to the waveguide modes, so-called pseudo modes may be distinguished. They carry infinite power, propagate mainly beyond the pore and decay quickly with growth of z in the soft range where the absorption is essential. They correspond to zeros in the denominator of the second fraction in (7) lying in the lower half-plane of the complex variable ρ in (8). Therefore, at $\lambda = 1.625$ and 17.06 nm, pseudo modes affect the field amplitude and phase/group velocity behavior only at low values of z, i.e. in the same place where the last term defining the transition processes in expression (8) is significant. With further propagation, the wave velocity behavior is defined only by ordinary waveguide modes.

However, in the hard X-ray radiation range $\lambda = 0.154\,\mathrm{nm}$, where the absorption is negligible, the role of pseudo modes is more significant. As may be shown by dispersion equation (9), near the cutoff threshold at $\varsigma \approx \pi n$, they propagate with velocities close to those in the continuous medium. For them $w_n \approx 1 - (\varsigma - \pi n)^2/2 \approx 1$, and their intensity inside the pore is π^2 times as high as that in the fundamental mode. Pseudo mode dominance when the absorption is low explains slow (compared with the law of fundamental mode dispersion) decrease in the phase velocity as the pore diameter grows at $\lambda = 0.154\,\mathrm{nm}$ as observed in Figure 2 on the left.

Conclusion

The study performs numerical simulation of the X-ray radiation propagation through narrow pores in PET track membranes in the $3D$-parabolic approximation. For numerical solution of the parabolic equation, the Crank–Nicolson type finite-difference scheme method with exact transparent boundary condition in a rectangular computational domain was used. The obtained field amplitudes for three wavelengths of both hard and soft X-ray radiation waves and for different pore diameters were used to calculate the phase and group velocities of waves propagating within the pore. It has been demonstrated that wave propagation usually takes place at constant group and phase velocity, in particular, in the range of hard X-ray radiation where the absorption is low. Velocity constancy is disturbed in case of propagation of several waveguide modes in the pore resulting in their interference and velocity oscillations. In the hard X-ray range, the product of the phase and group velocities is equal to squared speed of light in vacuum.

Using the analytical solution of the 2D parabolic equation by the integral transform method, a qualitative model of wave propagation in narrow pores was built. This model explains the main properties of wave velocities in pores, in particular, weak dependence of the phase and group velocities on the pore diameter in the hard X-ray radiation area.

The phase velocity constancy in pores found herein may be useful for creation of phase filters for X-ray radiation that change the field phase by a certain value. Since the phase velocity weakly depends on the pore diameter in the hard range, the X-ray radiation going through a porous membrane with the set thickness and different diameters of pores will acquire a fixed phase proportional to the membrane thickness. This phase will be independent on the angle of incidence of radiation on the membrane, but will depend on its wavelength. Much higher transmission of X-ray radiation will be the advantage of such filters compared with the solid polymer films. Phase filters based on track membranes may be, for example, used for chirping (i.e. X-ray radiation phase modulation such that it depends on the wavelength) of ultrashort X-ray pulses, including those from the free-electron laser. Pores in the track membranes may also serve as high-contrast precision test objects for examination of phase-contrast X-ray microscope properties and image restoration schemes [9].

Future studies are expected to investigate the phase and group velocity behavior of X-ray waves in non-cylindrical pores and in pores with rough interior walls. Numerical simulation of radiation propagation through the track membranes containing irregular pore arrays with different diameters and investigation of field phase modulation after propagation through such complex object are expected.

Acknowledgments

The authors are grateful to V.A. Bushuev for informative discussions on the properties of waves propagating in pores.

Funding

The study was supported financially by the Russian Federation represented by the Ministry of Science and Higher Education, agreement No. 075-15-2021-1350 dated October 5, 2021 (reference number 15.SYN.21.0004).

Conflict of interest

The authors declare that they have no conflict of interest.

References

[1] P.Yu. Apel, S.N. Dmitriev. *Trekovye membrany* V kn. A.B. Yaroslavtsev (red.). Membrany i membrannye tekhnologii (Nauchny mir, M., 2013), s. 117–160.
[2] M. Dominique, A.V. Mitrofanov, J.F. Hochedez, P.Y. Apel, U. Schühle, F.A. Pudonin, A. BenMoussa. Appl. Opt., **48** (5), 834 (2009). DOI: 10.1364/AO.48.000834
[3] A.V. Mitrofanov. Quant. Electron., **48** (2), 105 (2018). DOI: 10.1070/QEL16540
[4] A.V. Mitrofanov, P.Yu. Apel. Nucl. Instr. Meth. B, **245**, 332 (2006). DOI: 10.1070/QEL16540
[5] A.V. Mitrofanov, P.Yu. Apel. Izvestiya RAN. Ser. Fiz., **73** (1), 61 (2009) (in Russian).
[6] V.D. Kuznetsov (red.) *Solnechno-zemnaya fizika: Rezultaty eksperimentov na sputnike KORONAS-F* (Fizmatlit, M., 2009), s. 73. (in Russian)
[7] A.V. Mitrofanov, A.V. Popov, D.V. Prokopovich. Tech. Phys., **65** (11), 1814 (2020). DOI: 10.1134/S1063784220110195
[8] A.V. Mitrofanov, A.V. Popov, D.V. Prokopovich. Radioelektronika. Nanosistemy. Informatsionnyie tekhnolgii, **12** (2), 173 (2020) (in Russian). DOI: 10.17725/rensit.2020.12.173
[9] L. Brillouin. *Wave Propagation and Group Velocity* (Academic Press, 2013), v. 8.
[10] P.D. Gasparyan, F.A. Starikov, A.N. Starostin. Phys. Usp., **41** (8), 761 (1998). DOI: 10.1070/PU1998v041n08ABEH000428
[11] A.V. Mitrofanov, R.M. Feshchenko. *Kvantovaya elektronika*, 2024 (v pechati) (in Russian)
[12] M. Born, E. Volf. *Osnovy optiki* (Nauka, M., 1973) (in Russian)
[13] A.V. Mitrofanov, R.M. Feshchenko. Bull. Lebedev Phys. Institute, **49** (6), 169 (2022). DOI: 10.3103/S1068335622060057
[14] R.M. Feshchenko, A.V. Popov. JOSA A., **28** (3), 373 (2011). DOI: 10.1364/JOSAA.28.000373
[15] X-Ray Interactions with Matter, 2010. URL: www.cxro.lbl.gov/optical_constants/

Translated by E.Ilinskaya